ACADEMIA ROMÂNĂ
Revue Roumaine de Chimie
https://www.icf.ro/rrch/

Rev. Roum. Chim.,
2026, *71*(5–6), 363–372
DOI: 10.33224/rrch.2026.71.5-6.07

ANTIBACTERIAL ASSESSMENT AND CHARACTERIZATION OF MAGNESIUM OXIDE NANOPARTICLES SYNTHESIZED *VIA* CHEMICAL AND PHYTOSYNTEHSIS METHODS

Arshad HUSSAIN WAZIR,[*a] Bushra GUL,[b] Nabeel AHMAD[a] and Khurram Yaqoob[c]

[a]Carbon Materials Laboratory, Department of Chemistry, University of Science and Technology Bannu, Bannu-28100, Khyber Pukhtunkhwa, Pakistan
[b]Department of Biotecnology, University of Science and Technology Bannu, Bannu-28100, Khyber Pukhtunkhwa, Pakistan
[c]School of Chemical and Materials Engineering (SCME), National University of Science and Technology (NUST), H-12, Islamabad, Pakistan

Received March 27, 2025

This study explores the synthesis and antibacterial properties of magnesium oxide nanoparticles (MgO NPs) using chemical and phytosynthesis methods. Chemically synthesized MgO NPs were produced from magnesium sulfate and sodium hydroxide, while phytosynthesis as green method utilized *Curcuma longa* Linn *(C. longa)* extract. Characterization techniques such as UV-Vis, FT-IR, XRD, and SEM confirmed their structural and morphological properties. UV-Vis spectra showed absorption peaks at 284.5 nm and 316.5 nm, while XRD confirmed crystallinity, with average crystallite sizes of 14.5 ± 1.6 nm for phytosynthesized MgO NPs and 20.8 ± 2.3 nm for chemically synthesized MgO NPs. SEM analysis revealed that chemically synthesized MgO NPs form dense, smooth, quasi-spherical agglomerates, whereas phytosynthesized MgO NPs exhibit rough, irregular particles with loosely packed and porous structures. Antibacterial activity was tested against *E. coli*, *K. pneumoniae*, and *S. cereus*, with phytosynthesized MgO NPs exhibiting superior efficacy. These findings emphasize the influence of synthesis methods on the physicochemical and biological properties of MgO NPs, reinforcing their potential for antibacterial applications.

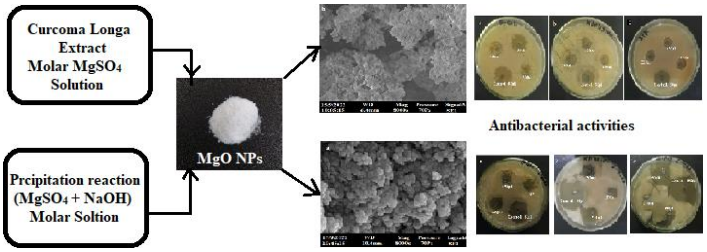

INTRODUCTION

MgO NPs hold significant importance due to their versatile applications in areas like nanotechnology, material science, and biomedical research. Their value arises from unique characteristics of high photocatalytic efficiency, high chemical and thermal stability, excellent surface area, anticancer properties and strong antimicrobial activity.[1–5] Among their many applications, the antimicrobial activity of MgO NPs is particularly notable. This activity is primarily due to their capability of producing reactive oxygen species on their surfaces that result in damaging bacterial cell walls, protein denaturation, and disruption of crucial cellular functions.[6] As a result,

[*] Corresponding author: arshadwaziri@gmail.com; ORCID: http://orcid.org/0000-0001-7473-1429

MgO NPs are highly effective against a broad range of bacteria, including antibiotic-resistant strains. These characteristics make them a promising alternative to conventional antibiotics and other antibacterial agents, especially as resistance to standard treatments increases.[7]

The synthesis method is vital in defining the physicochemical characteristics of MgO NPs, including size, shape, surface area, and crystallinity, all of which affect their antibacterial effectiveness. Chemical synthesis approaches like sol-gel, co-precipitation, and solution combustion are known to produce MgO NPs with controlled size and high purity, making them suitable for applications requiring strong crystallinity and stability.[8–10] However, these chemical methods often use toxic reagents and generate harmful by-products, raising environmental concerns and limiting their suitability for biomedical applications where biocompatibility is crucial.[11]

To overcome these challenges, green synthesis methods have been developed that use natural resources like fungi, bacteria and extracts of plants for reduction and stabilization purposes to produce MgO NPs.[12,13] Unlike chemical synthesis, green methods are environmentally friendly and generally yield biocompatible nanoparticles suitable for medical and agricultural use.[14] Plant-based synthesis (phytosynthesis) is particularly advantageous due to the abundance of bioactive compounds (such as alkaloids, phenolic compounds, terpenoids, glycosides, saponins, and etc.**)** in plant extracts, which act as natural capping agents, enhancing the stability and functionality of MgO NPs.[15] Additionally, green-synthesized MgO NPs often demonstrate properties comparable to or even superior to those produced through traditional chemical methods, particularly in terms of lower cytotoxicity and greater antimicrobial efficacy against pathogenic bacteria.[16]

Using the methods mentioned, various strategies have been employed to synthesize MgO NPs. For example, MgO NPs were prepared by reacting magnesium sulfate with sodium hydroxide, forming a magnesium hydroxide precipitate, The precipitate was converted to MgO NPs under heat treatment and were characterized with different techniques.[17] Suresh *et al*.[18] synthesized MgO NPs using magnesium nitrate, sodium hydroxide (as precursors) and starch (as stabilizer). The product was characterized by XRD and SEM, and also evaluated their antibacterial effects against *S. aureus and E. coli*. Sim *et al*.[19] applied a sol-gel method to prepare MgO NPs to find superior antibacterial activity against *Serratia* and *Streptococcus* compared to commercial NPs. Abinaya and Helen[20] compared hydrothermal, green, microwave, and sol-gel methods for synthesizing MgO NPs, showing hydrothermally derived NPs to be the most effective against both bacterial strains and *Aedes* mosquito larvae. Fouda *et al*.[21] used *Punica granatum* peel extract to synthesize MgO NPs, which exhibited significant antimicrobial activity against *Bacillus subtilis*, *S. aureus*, *E. coli*, *Pseudomonas aeruginosa*, and *Candida albicans*, as well as larvicidal activity against *Culex quinquefasciatus* larvae, highlighting their potential for dual antimicrobial and larvicidal applications.

The green synthesis of MgO NPs using plant extracts has attracted considerable interest due to its environmentally friendly and cost-effective nature. MgO NPs synthesized with extracts from *Sedum morganianum*, *Sansevieria trifasciata*, *Echeveria elegans*, and *Aloe vera* have shown potential in bone implant applications, exhibiting good thermal stability, photocatalytic properties, and, notably, the first reported Surface-enhanced Raman scattering spectroscopy detection of L-phenylalanine.[22] Similarly, MgO NPs biosynthesized using *Hagenia abyssinica* extract were found to be spherical with a face-centered cubic structure (10–40 nm) and demonstrated significant antibacterial activity, particularly against *S. aureus* and *E. coli*.[23] Another study using *Justicia adhatoda* leaf extract produced crystalline, spherical MgO NPs (22.96 nm) that exhibited strong antimicrobial effects, surpassing the efficacy of Gentamicin at higher concentrations.[24] *Curcuma longa* L. (Family: Zingiberaceae), commonly called turmeric, is a rhizomatous perennial herb indigenous to tropical South Asia. The plant is distinguished by its fleshy rhizomes that exhibit a characteristic golden-yellow pigmentation due to curcuminoid content and widely used as medicine, foodstuff, and cosmetic.[25–27] Thereore, *C. longa* is considered to be rich in bioactive compounds such as curcumin and has been successfully employed in the phytosysynthesis of metal/metal oxide NPs.[28,29] The presence of natural capping and reducing agents in turmeric enhances the stability and biological activity of the resulting nanoparticles.[30,31]

Research has shown that phytosynthesized MgO NPs demonstrate strong antibacterial activity against a wide range of bacterial strains. Wherein, their antimicrobial mechanism is generally

attributed to the production of reactive oxygen species (ROS), direct damage to cell membranes, and enhanced bioactivity from residual plant-derived compounds on the nanoparticle surface.[32,33] These features often make phytogenic MgO NPs more efficient and biocompatible than those synthesized through conventional chemical pathways. Recent studies have also demonstrated that the size and morphology of green-synthesized MgO NPs significantly influence their antibacterial performance. MgO NPs produced using Bauhinia variegata leaf extract exhibited an average size of 13 nm with a face-centered cubic structure, showing strong antibacterial effects against *E. coli*, *S. aureus*, and *Salmonella* species.[34] Similarly, fungal-mediated MgO NPs synthesized by *Aspergillus terreus* ranged from 8–38 nm, displaying high antimicrobial efficacy against multiple pathogens, including *S. aureus* and *P. aeruginosa*, with notable growth inhibition at 200 µg/mL.[35] Furthermore, MgO NPs synthesized from orange peel extract were around 9–40 nm in size and showed effective activity, particularly against Gram-positive bacteria and *Pseudomonas aeruginosa* biofilms, while maintaining good cytocompatibility. Generally, smaller MgO NPs (8–20 nm) exhibit enhanced antibacterial and catalytic activities, attributed to their high surface area, crystalline structure, and phytochemical-mediated stabilization, making them promising for biomedical and environmental applications.[36]

The present study investigates the chemical and phytosynthesis processes of MgO NPs and determines their antibacterial efficacy toward two Gram– bacteria (*E. coli* and *K. pneumoniae*) and one Gram+ bacterium (*S. aureus*) that aims to compare how the preparation method affects their performance. Detailed characterization using XRD, SEM, UV-Vis and FTIR is also performed to analyze their structures, sizes and surface chemistry.

EXPERIMENTAL

Materials

Analytical grade chemicals were purchased from Sigma-Aldrich such as magnesium sulphate ($MgSO_4$), caustic soda (NaOH), bismuth nitrate ($Bi(NO_3)_3$) tartaric acid or 2, 3-dihydroxybutanedioic acid ($C_4H_6O_6$), potassium iodide (KI), magnesium chips, hydrochloric acid (HCl), Iron(III) chloride ($FeCl_3$), Gelatin $C_6H_{12}O_6$), sulphuric acid (H_2SO_4), chloform (CHC_{l3}), ammonia (NH_3). Deionized water was used in all experiments.

Extract preparation

Turmeric (*C. longa*) roots were obtained from a locally cultivated area of District Bannu (Surani), Khyber Pakhtunkhwa, Pakistan. To prepare the extract, the roots were thoroughly washed with distilled water and then dried in an oven at 60 °C overnight. The dried roots were ground into a fine powder. Fifty grams of the powdered root material were mixed with deionized water (500 mL) and heat treated for 30 minutes at 100 °C. The mixture was then allowed to incubate at room temperature overnight. Finally, filtration of the concentrate was performed to collect the extract and stored up for further use in the experiment in a refrigerator at 4 °C.

Phytochemical Analysis of *C. longa*

The presence of major phytoconstituents in *C. longa* extracts was verified by standard qualitative assays in which specific reagent reactions produce characteristic colour changes in the test mixtures. Using established protocols, the extracts were screened and found to contain alkaloids, curcuminoids, flavonoids, phenolics, saponins, tannins, and terpenoids.[37,38]

Synthesis of MgO NPs

Chemical Synthesis of MgO NPs

To synthesize MgO NPs separate homogeneous molar solutions of 0.83 M $MgSO_4$ and 1 M NaOH were prepared in deionized water. These solutions were then combined to stir for 2 h. After filtration and washing processes, the resulting magnesium hydroxide ($Mg(OH)_2$) precipitate was dried in an oven at 105 °C for 2 h. Subsequently, Carbolite AAF-1100 Ashing Furnace was used to sinter the product at 300 °C for 3 h, yielding MgO NPs. The final product was transferred to a glass vial and stored in a desiccator for further analysis. The conversion of $Mg(OH)_2$ to MgO NPs is demonstrated by the reactions shown in equations (eq. 1) and (eq. 2).

$$2NaOH_{(aq)} + MgSO_{4(aq)} \rightarrow Na_2SO_{4(aq)} + Mg(OH)_{2(s)} \quad (1)$$

$$Mg(OH)_2 \rightarrow MgO + H_2O \quad (2)$$

Phytosynthesis of MgO NPs

MgO NPs were also synthesized using photosynthesis as green method. In this process, 10 ml of *C. longa* extract was mixed with an aqueous solution of 0.1 molar $MgSO_4$ (50 ml) and was kept under stirring for 6 h at 80 °C. During the stirring process, a 1 M NaOH solution in deionized water was added drop wise to the reaction mixture to achieve the desired pH, promoting the formation of $Mg(OH)_2$. Wherein, the pH was maintained at 10.5. After the reaction time was complete, the mixture was centrifuged at 5000 rpm for 10 minutes. After drying at 105 °C in oven for 2 h, the collected material was further sintered in a Furnace (Carbolite AAF-1100) at 450 °C for 3 h to produce MgO NPs, which were stored for analysis.

Characterization

The obtained MgO NPs were characterized with various techniques. Ultraviolet-Visible (UV-1800 Shimadzu, Japan) spectroscopic analysis was conducted to evaluate their absorption peaks. Infrared spectroscopy (Eco-ATR Spectrometer, Alpha, Bruker) was performed to analyze the surface functionalities of the products. Scanning electron microscopy (SEM) (Model-JSEM5910 JEOL-Japan) was used to identify the morphology of MgO NPs.

X-ray diffractometer (model JDX-3532 JEOL, Japan) with CuKα radiation (λ=1.5418 Å) was used for analysis of phase transformations and crystal structure. The particle size of the MgO NPs was calculated using the Scherrer equation:

$$d = \frac{K\lambda}{\beta \cos \theta}$$

wherein, K= (typically 0.9) Scherrer constant, λ= wavelength, β= FWHM (full width at half maximum) in radians, θ= Bragg angle and d= particle size.

Antibacterial Assessment

The synthesized MgO NPs via green and chemical methods were evaluated against three bacterial strains: *Staphylococcus aureus* (*S. aureus)* Gram-positive (Gram+), *Klebsiella pneumoniae* **(**K. *pneumonia***)** and *Escherichia coli* **(***E. coli***)** Gram-negative (Gram–) for their antibacterial activities. The agar well diffusion method, a well-established technique for assessing antibacterial susceptibility, was employed for this purpose.[22,23,39,40] The bacterial cultures were obtained from the Microbiology Lab of the University of Science and Technology Bannu and maintained on nutrient agar slants to ensure viability. Fresh inocula were prepared by nutrient broth culturing the bacteria and incubating for 18 to 24 h under heat treatment of 37 °C. Mueller-Hinton Agar (MHA) was used as the growth medium for the antibacterial assay. An autoclave was used to heat 3 g of agar in 150 mL of deionized water at 15 lbs of pressure and 121 °C for 15 minutes and then its temperature was reduced to 55 °C – 60 °C before being poured into sterile petri dishes within a laminar air flow cabinet. After the dishes solidified, the 24-hour-old bacterial cultures were evenly swabbed onto the agar surface using sterile cotton swabs. Wells were created in the center of each quadrant of the Petri plates using a sterile pipette tip. Different concentrations of the green and chemically synthesized MgO NPs (150 µg/mL, 200 µg/mL, and 250 µg/mL) were then introduced into the wells using a micropipette. Ciprofloxacin (1 mg/mL) was used as a positive control. The plates were incubated at 37 °C for 24 hours, and the formation of inhibitory zones around the sample wells was observed, indicating the nanoparticles antibacterial activity. The diameters of the inhibitory zones were measured in millimeters (mm), and the average values were calculated from triplicate experiments. The study utilized both Gram+ (*S. cereus*) and Gram– (*K. pneumonia* and *E. coli*) bacterial strains to comprehensively evaluate the antibacterial efficacy of the synthesized MgO NPs. This selection is crucial because the two classes of bacteria have fundamentally different cell wall structures. The thick, peptidoglycan-rich layer of Gram-positive bacteria and the complex, multi-layered outer membrane of Gram-negative bacteria result in differing permeability to antibacterial agents. By testing against both types, the research can determine if the MgO NPs have a broad-spectrum effect or if their activity is selectively more potent against one class, providing a more complete understanding of their potential application.

RESULTS AND DISCUSSION

Phytochemical screening of *C. longa*

Qualitative phytochemical screening of *C. longa* rhizome extract revealed a broad spectrum of bioactive compounds, including alkaloids (Dragendorff's test), curcuminoids (borax-HCl test), flavonoids (Shinoda test), phenolic compounds (Folin–Ciocalteu assay), saponins (foam test), tannins (ferric-chloride test), and terpenoids (Salkowski test), as summarized in Table 1.[37,38] These phytochemicals

endow the extract with strong redox potential, enabling it to function as a natural reducing and stabilizing medium during the green synthesis of metal-oxide nanoparticles.[41]

In the case of MgO NPs, the phytochemical constituents of *C. longa*, particularly phenolics, curcuminoids, and flavonoids chelate Mg^{2+} ions from precursor salt ($MgSO_4$) through oxygen-containing functional groups such as hydroxyl and carbonyl.[42,43] Upon heating, these bio-reductants undergo oxidation, releasing electrons that reduce the chelated Mg^{2+} ions to magnesium hydroxide [$Mg(OH)_2$] intermediates, which subsequently dehydrate or calcine to yield crystalline MgO NPs.[44] Concurrently, terpenoids and saponins adsorb on the growing nuclei, acting as capping and stabilizing ligands that regulate particle size, morphology, and colloidal stability by preventing aggregation.[36] This dual functionality, reduction and stabilization of plant extarct-derived phytochemicals underlie their efficacy in the eco-friendly synthesis of MgO and other metal-oxide nanomaterials.[45]

Table 1

Preliminary phytochemicals analysis of *C. longa* extract

S. No.	Phytochemicals	Extract content
1	Alkaloids	+
2	Curcumin Tannins	+
3	Flavonoids	+
4	Glycosides	–
5	Phenolics	+
6	Saponins	+
7	Tannins	+
8	Terpenoids	+

'–' = absence, '+' = presence

Characterization of the MgO NPs

UV-Vis spectra of the MgO NPs synthesized through chemical and plant-phytosynthesized approaches (Fig. 1) show absorption peaks at around 316.5 nm and 284.5 nm. These peaks arise from electronic transitions within MgO and fall within the range commonly reported for nanosized MgO structures prepared using green and conventional methods.[3,46,47] Earlier studies, such as those involving *Bauhinia variegata* extracts, biosynthesized MgO NPs used for catalytic and antimicrobial applications, brown-seaweed–derived MgO, and other plant-assisted syntheses have similarly observed absorption bands between 280 and 330 nm, confirming that the obtained spectra are characteristic of MgO at the nanoscale.[48–52]

The more pronounced blue shift in the *C. longa* extract synthesized sample suggests a little smaller particle size than that of the chemically synthesized nanoparticles, which is consistent with findings that phytochemicals can act as natural stabilizers and produce finer MgO particles[5]. Under UV illumination (365 nm), both nanoparticle solutions emitted a clear blue fluorescence (inset, Fig. 1), a behavior often attributed to surface or defect-related states such as oxygen vacancies, as also discussed in recent green-synthesis studies.[50,52] In general, the observed absorption and fluorescence features closely match established trends in the literature, supporting the successful formation of MgO NPs *via* both synthetic routes.

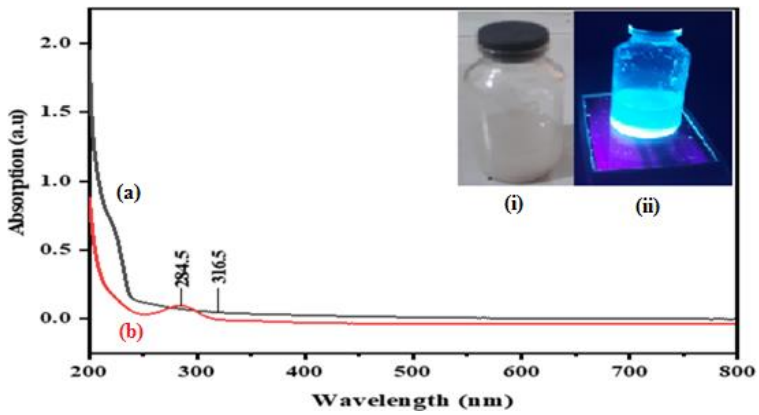

Fig. 1 – UV profile of the MgO NPs prepared by (a) chemical and (b) phytosynthesis methods, and its optical views of fluorescence images under (I) Visible light and (II) UV light.

Figures 2 (a) and (b) depict the FTIR analyses of MgO NPs prepared through chemical and phytosynthetic routes, confirming successful MgO formation and revealing differences in surface chemistry. In both samples, characteristic absorption bands appear in the 400–700 cm^{-1} region ranges, corresponding to Mg–O stretching vibrations, which are widely recognized as the

fingerprint region of MgO NPs. The chemically synthesized MgO exhibits a strong band at 529 cm^{-1}, whereas the phytosynthesized MgO shows a corresponding band near 654 cm^{-1}, in good agreement with reported MgO NPs obtained through both chemical and green routes.[53,54]

The high wave number region range (3100–3900 cm^{-1}) provides insight into surface hydroxylation. The chemically synthesized MgO shows weak bands at 3904–3805 cm^{-1} and a minor feature near 3147 cm^{-1}, attributed to residual surface –OH groups and adsorbed moisture, indicating effective removal of hydroxyl species during calcination at 300 °C.[55,56] In contrast, the phytosynthesized MgO displays broader and more intense O–H stretching bands at 3877, 3776, and 3711 cm^{-1}, with a shoulder at 3046 cm^{-1}, reflecting higher surface hydroxylation and hydrogen-bonded species derived from *C. longa* phytochemicals. Such features are commonly reported for green-synthesized MgO NPs due to plant-mediated surface stabilization.[57,58] Additional absorption in the 1000–1700 cm^{-1} region observed for the phytosynthesized MgO is assigned to C–O, C–H, and C=O vibrations of residual biomolecules, confirming phytochemical capping of the nanoparticles.[59,60] These organic signatures are largely absent in the chemically synthesized MgO, which shows only a weak 2357 cm^{-1} band attributed to atmospheric CO_2 and a low-intensity feature near 1524 cm^{-1}, commonly associated with surface absorption of CO_3^{2-} (carbonate ions).[61,62]

On the whole, FTIR results confirm that both synthesis routes yield MgO NPs via thermal decomposition of $Mg(OH)_2$. However, the phytosynthesized MgO retains additional hydroxylated and organic surface functionalities due to *C. longa* -extract mediation, whereas the chemically synthesized MgO exhibits a cleaner oxide surface. These differences in surface chemistry may influence catalytic, adsorption, and antibacterial behavior.

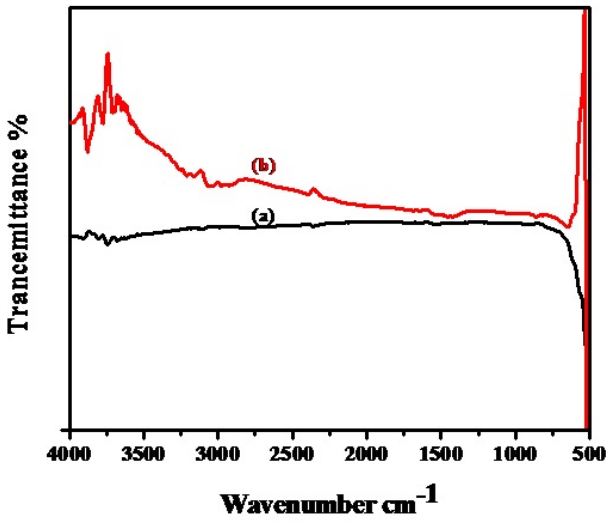

Fig. 2 – FT-IR profile of the MgO NPs produced by (a) chemical and (b) phytosynthesis methods.

Figures 3(a) and (b) present the XRD patterns of MgO NPs synthesized by chemical and phytosynthesis routes. For both samples, the prominent diffraction peaks are observed within the 2θ range of 20°–80°. The diffraction peaks appearing at approximately 36.8–36.9°, 42.8–42.9°, 62.2–62.3°, 74.6–74.7°, and 78.5–78.6° are indexed to the (111), (200), (220), (311), and (222) crystallographic planes of the face-centered cubic MgO structure, respectively, confirming the crystalline nature of the synthesized nanoparticles. These reflections are in good agreement with the standard diffraction pattern of cubic MgO (ICDD file No. 45-0946).[63–65] A clear difference in peak broadening is evident between the chemically synthesized and phytosynthesized MgO NPs. The relatively broader diffraction peaks observed for the phytosynthesized MgO indicate a smaller crystallite size compared to the chemically synthesized sample. The average crystallite size, calculated using the Debye–Scherrer equation, was determined to be 14.5 ± 1.6 nm for phytosynthesized MgO NPs and 20.8 ± 2.3 nm for chemically synthesized MgO NPs, which is consistent with previously reported crystallite size ranges for green- and chemically synthesized MgO NPs.[66–68] The corresponding XRD peak positions, FWHM values, and calculated crystallite sizes are summarized in Table 2.

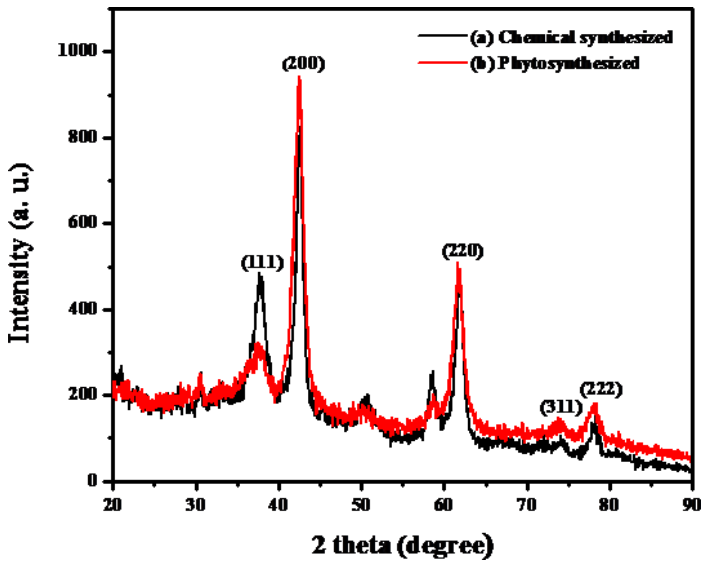

Fig. 3 – XRD pattern of MgO NPs synthesized by (a) chemical and (b) phytosynthesis processes.

Table 2

XRD peak positions, FWHM, and crystallite sizes of MgO NPs.

	2θ (°)	FWHM	Crystallite size (nm)	hkl
Chemically Synthesized				
MgO NPs	36.9	0.38	22.4	(111)
	42.9	0.35	24.1	(200)
	62.3	0.42	20.6	(220)
	74.7	0.46	18.9	(311)
	78.6	0.48	18.1	(222)
Average crystallite size			20.8 (± 2.3)	
Phytosynthesized				
MgO NPs	36.8	0.55	15.4	(111)
	42.8	0.51	16.9	(200)
	62.2	0.60	14.3	(220)
	74.6	0.65	13.2	(311)
	78.5	0.67	12.8	(222)
Average crystallite size			14.5 (± 1.6)	

SEM microphotographs in Figs. 4(a) and (b) illustrate the surface morphology of the obtained MgO NPs, recorded at a magnification of 8000× with working distances of approximately 10.4 mm for chemically synthesized MgO and 6.4 mm for phytosynthesized MgO. The chemically synthesized MgO NPs (Fig. 4a) exhibit a quasi-spherical morphology forming dense and compact agglomerates with relatively smooth surfaces and low porosity. Such features are typical of chemical synthesis routes, where rapid nucleation and limited organic surface capping promote close particle packing and compact aggregation.[68–70] In contrast, the phytosynthesized MgO NPs (Fig. 4b) display irregular to nearly spherical particles arranged in loosely packed, porous agglomerates with rough and heterogeneous surfaces. This morphology is characteristic of green synthesis methods, in which plant-derived phytochemicals act as reducing and capping agents, influencing particle growth and enhancing surface porosity.[71,72] Similar porous and agglomerated structures have been reported for MgO NPs synthesized using plant extracts such as *Verbascum sinaiticum*, *Lawsonia inermis*, and *Bauhinia variegata*.[71–73] The agglomeration observed in both samples is mainly attributed to the high surface energy of MgO NPs, which induces clustering through electrostatic and van der Waals interactions. However, chemically synthesized MgO forms more compact aggregates, whereas phytosynthesized MgO develops more open and porous networks due to the presence of phytochemicals on the particle surface.[68,74,75] Overall, the SEM results confirm that the synthesis route strongly influences MgO NPs morphology, in agreement with reported literature.[68–75]

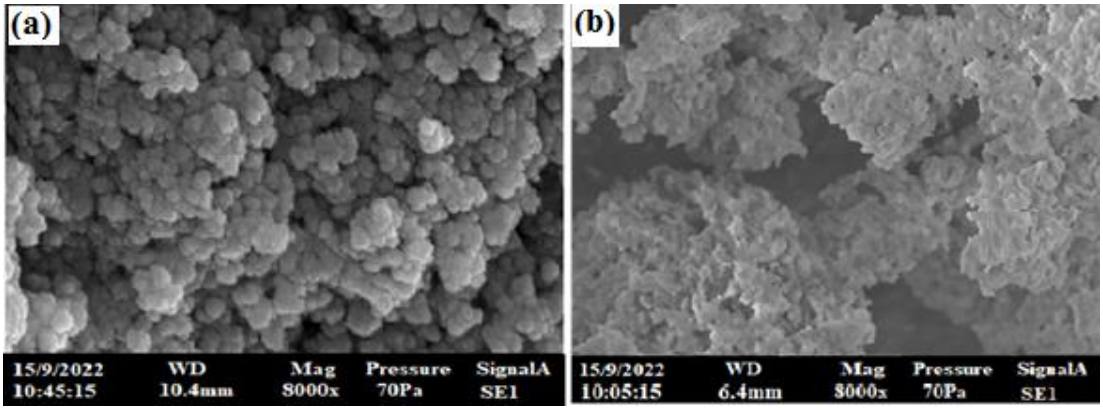

Fig. 4 – Micrographs of MgO NPs obtained by (a) chemical and (b) phytosynthesis methods.

Antibacterial activity

Table 3 summarizes the antibacterial effects against selected bacterial strains of both the obtained MgO NPs by chemical and phytosynthesis methods. These effects were evaluated against *K. pneumonia*, *E. coli* and *S. aureus*. Similarly, the Figs. 5 (a–c) and (d–f) illustrate the inhibition zones for *E. coli*, *K. pneumoniae* and *S. aureus* at varying concentrations of MgO NPs, with ciprofloxacin serving as a control. Results demonstrate significant antibacterial activity by MgO NPs, with phytosynthesized NPs exhibiting more potent inhibitory effects compared to chemically synthesized counterparts. The concentration dependent antibacterial activity of both the chemically and biologically synthesized MgO NPs was recorded. At 250 µg/mL MgO NPs showed significantly greatest antibacterial activity against *E. coli*, *K. pneumoniae* and *S. cereus*. The negative control *i.e*. pure DMSO showed no antibacterial activity against all the tested bacteria.

The observed antibacterial activity can be attributed to multiple mechanisms. First, MgO NPs generate ROS upon interaction with bacterial cells, leading to oxidative stress and subsequent cellular damage.[75] Additionally, the nanoscale size of MgO NPs allows them to interact with and disrupt bacterial cell membranes directly, causing leakage of intracellular contents and impairing cell function.[19] Lastly, the MgO NPs may release magnesium ions in the bacterial environment, which could interfere with cellular metabolic processes essential for bacterial survival.[1] Collectively, these mechanisms underline the enhanced antibacterial efficacy observed with MgO NPs obtained by phytosynthesis method.

Table 3

Antibacterial activities of MgO NPs against pathogenic bacterial strains

Treatments	Zone of inhibition (mm)		
	E. coli	***K. pneumoniae***	***S. cereus***
Chemically synthesized MgO NPs			
Ciprofloxacin 50 µg/mL	30±0.60^{a}	28 ±0.01^{a}	29 ±1.64^{a}
MgO NPs (1). 150 µg/mL	19±0.54^{c}	20 ±0.0^{c}	17 ±0.57^{d}
(2). 200 µg/mL	21±0.69^{c}	24 ±0.04^{b}	22 ±0.0^{c}
(3). 250 µg/mL	28±0.75^{a}	29 ±0.0^{c}	32 ±0.0c
DMSO	0.0±0.0^{d}	0.0 ±0.0^{d}	0.0 ±0.0^{e}
Green synthesized MgO NPs			
Ciprofloxacin 50 µg/mL	31 ±0.55^{a}	44 ±0.48^{a}	45 ±0.95a
MgO NPs (1). 150 µg/mL	20 ±1.51^{b}	22 ±0.27^{d}	21 ±0.14^{d}
(2). 200 µg/mL	28 ±0.75^{a}	29 ±0.0^{c}	32 ±0.0^{c}
(3). 250 µg/mL	30 ±0.0^{a}	36 ±1.12^{b}	37 ±0.19^{b}
DMSO	0.0 ±0.0^{c}	0.0 ±0.0^{e}	0.0 ±0.0^{e}

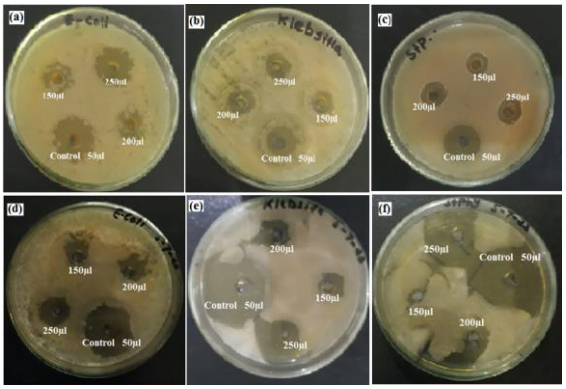

Fig. 5 – Inhibition zone of MgO NPs produced by chemical (a–c) and phytosynthesis methods (d–f) on *K. pneumoniae*, *E. coli* and *S. aureus* by varying concentrations of MgO NPs and control drug Ciprofloxacin.

CONCLUSION

This work demonstrates that the synthesis route plays a decisive role in governing the physicochemical characteristics and antibacterial performance of MgO NPs. Both chemical and phytosynthesis methods successfully produced crystalline MgO NPs; however, phytosynthesized MgO NPs derived from *C. longa* extract exhibited smaller crystallite size, higher surface hydroxylation, and more porous morphology compared to chemically synthesized counterparts. These structural and surface features translated directly into enhanced antibacterial activity against Gram– (*E. coli*, *K. pneumoniae*) and Gram+ (*S. cereus*) bacteria, particularly at higher nanoparticle concentrations. The superior efficacy of phytosynthesized MgO NPs is attributed to their reduced particle size, increased surface reactivity, and the presence of plant-derived functional groups that promote stronger interactions with bacterial cell membranes and oxidative stress mechanisms. Collectively, this study highlights phytosynthesis as an environmentally benign, cost-effective, and efficient strategy for producing MgO NPs with improved antibacterial functionality, underscoring their strong potential for future biomedical and antimicrobial applications.

REFERENCES

1. M. Fernandes, K. R. B. Singh, T. Sarkar, P. Singh and R. P. Singh, *Adv. Mater. Lett.*, **2020**, *11*, 1.
2. D. Gingaşu, I. Mîndru, D. C. Culiță, L. Predoană, G. Petcu, M. Ciobanu, S. Preda, J. Pandele-Cuşu and S. Petrescu, *Rev. Roum. Chim.*, **2021**, *66*(5), 463–473.
3. R. B. Rotti, D. V. Sunitha, R. Manjunath, A. Roy, S. B. Mayegowda, A. P. Gnanaprakash and E. B. Khidir, *Front. Chem.*, **2023**, *11*, 1143614.
4. Y. He, S. Ingudam, S. Reed, A. Gehring, T. P. Strobaugh and P. Irwin, *J. Nanobiotechnol.*, **2016**, *14*, 54.
5. R. Periakaruppan, V. Naveen and J. Danaraj, *JOM*, **2022**, *74*, 4817.
6. W. Ahmad and S. Kumar, *Emergent Mater.*, **2024**, *7*, 1081.
7. N. Beyth, Y. Houri-Haddad, A. Domb, W. Khan and R. Hazan, *eCAM*, **2015**, *1*, 246012.
8. H. Hemmami, I. B. Amor, S. Zeghoud, S. E. Laouini, E. Nleonu, P. Pohl and J. Simal-Gandara, *J. Turk. Chem. Soc. A: Chem.*, **2024**, *11*, 731.
9. M. Mehta, M. Mukhopadhyay, R. Christian and N. Mistry, *Powder Technol.*, **2012**, *226*, 213.
10. K. Tharani, A. J. Christy, S. Sagadevan and L. C. Nehru, *Chem. Phys. Lett.*, **2021**, *763*, 138216.
11. S. Rani, P. Kumar and N. Kataria, *J. Taiwan Inst. Chem. Eng.*, **2024**, *166*, 105566.
12. M. H. M. Edwin, S. A. Sundara Raj, A. Mani, M. Sillanpää and S. Al-Farraj, *Nanotechnol. Rev.*, **2024**, *13*, 20240048.
13. A. I. Humaira, H. A. Shakir, M. Khan, S. Ali, M. Alshahrani and M. Irfan, *Chem. Bio. Eng. Rev.*, **2024**, *11*, 447.
14. P. Sathiya and G. Kannappan, *Inorg. Nano-Met. Chem.*, **2023**, *1*, 1.
15. J. O. Adeyemi, A. O. Oriola, D. C. Onwudiwe and A. O. Oyedeji, *Biomolecules*, **2022**, *12*, 627.
16. A. A. Silva, A. M. F. Sousa, C. R. Furtado and N. M. Carvalho, *Mater. Today Sustain.*, **2022**, *20*, 100203.
17. M. Mehta, M. Mukhopadhyay, R. Christian and N. Mistry, *Powder Technol.*, **2012**, *226*, 213.
18. J. Suresh, R. G. R. Gandhi, S. Selvam and M. Sundrarajan, *Adv. Mater. Res.*, **2013**, *678*, 297.
19. H. T. Sim, M. Gençaslan and M. Merdan, *Discov. Appl. Sci.*, **2024**, *6*, 1.
20. S. Abinaya and H. P. Kavitha, *ACS Omega*, **2023**, *8*, 5225.
21. A. Fouda, K. S. Alshallash, M. I. Alghonaim, A. M. Eid, A. M. Alemam, M. A. Awad and M. F. Hamza, *Chemistry*, **2023**, *5*, 2009.
22. E. Proniewicz, A. M. Vijayan, O. Surma, A. Szkudlarek and M. Molenda, *Int. J. Mol. Sci*., **2024**, *25*, 4242.
23. B. Y. Hirphaye, N. B. Bonka, A. M. Tura and G. M. Fanta, *Appl. Water Sci.*, **2023**, *13*, 175.
24. K. K. Ilavenil, V. Senthilkumar, A. Kasthuri and S. Sivaraman, *Mater. Today Proc.*, **2024**. https://doi.org/10.1016/j.matpr.2024.05.144
25. J. Leong-Škorničková, O. Šida, S. Wijesundara and K. Marhold, *Bot. J. Linn. Soc.*, **2008**, *157*, 37–46.
26. E. J. Iweala, M. E. Uche, E. D. Dike, L. R. Etumnu, T. M. Dokunmu, A. E. Oluwapelumi, B. C. Okoro,O. E. Dania, A. H. Adebayo and E. A. Ugbogu, *Pharmacol. Res.- Mod. Chin. Med*., **2023**, *6*, 100222.

27. K. Sulaymanov, P. Johri, A. Azimov, A. Narimanov, F. Kodiralieva, S. Singh and D. Jabborova, *Turk J. Agric. For.*, **2024**, *8*, 647–657.
28. F. K. Alsammarraie, W. Wang, P. Zhou, A. Mustapha and M. Lin, *Colloids Surf. B: Biointerfaces*, **2018**, *171*, 398–405.
29. K. K. Ilavenil, V. Senthilkumar and A. Kasthuri, *Discov. Catal.*, **2025**, *2*, 3.
30. D. Patra and R. El Kurdi, *G. Chem. Lett. Rev.*, **2021**, *14*, 474–487.
31. A. Gangal, N. K. Sethiya, M. Duseja, R. K. Shukla, D. Bisht, V. S. Rana, H. . Lalhlenmawia, S. Azizov and D. Kumar, *G. Chem. Lett. Rev.*, **2025**, *18*, 2449122.
32. S. Vijayakumar, V. N. Punitha and N. Parameswari, *Arab. J. Sci. Eng*, **2022**, *47*, 6729–6734.
33. S. Mahalingam, A. K. Mani, D. Ali, S. Rengarajan, A. Angamuthu, A. Srinivasan, S. Bakthavatchalam and J. Kim, *Biomass Convers. Biorefin.*, **2024**, *14*, 30819–30831.
34. F. Aziz, A. B. Gulshan, Z. Usman, M. Rehman, Q. Khalid, M. N. Khan, M. U. Munir, H. T. Masood and M. Rafique, *Results Chem.*, **2025**, *15*, 102248.
35. E. Saied, A. M. Eid, S. E. D. Hassan, S. S. Salem, A. A. Radwan, M. Halawa, F. M. Saleh, H. A. Saad, E. M. Saied and A. Fouda, *Catalysts*, **2021**, *11*, 821.
36. D. M. Radulescu, I. A. Neacsu, B. S. Vasile, V. A. Surdu, O. C. Oprea, R. D. Trusca, C. Chircov, R. C. Popescu, C. I. Ilie, L. M. Ditu and V. Drumea, *Int. J. Mol. Sci.*, **2025**, *26*, 9021.
37. K. Sulaymanov, P. Johri, A. Azimov, A. Narimanov, F. Kodiralieva, S. Singh and D. Jabborova, *Turk. J. Agric. For.*, **2024**, *48*(5), 647–657.
38. Y. O. Zhran, Y. A. Ramadan, A. S. Farid and A. M. El-Mahmoudy, ***Science Archives,*** **2023**, *4*, 162–169
39. A. H. Wazir, Q. Khan, N. Ahmad, F. Ullah, I. Quereshi and H. Ali, *Korean J. Mater. Res.*, **2022**, *32*, 80.
40. A. H. Wazir, K. Qudratullah, A. Afaq and U. Inayat, *JOMALISC*, **2024**, *3*, 81.
41. S. Singaravelu, F. Motsoene, H. Abrahamse and S. S. Dhilip Kumar, *Front. bioeng. biotechnol.*, **2025**, *13*, 1637589.
42. S. Faisal, N. S. Al-Radadi, H. Jan, Abdullah, S. A. Shah, S. Shah, M. Rizwan, Z. Afsheen, Z. Hussain, M. N. Uddin and M. Idrees, *Coatings*, **2021**, *11*, 849.
43. O. C. YILDIRIM and H. TÜRKEZ, Green Synthesis of Magnesium Oxide Nanoparticles by Using Petroselinum crispum Extract and Their Potent Antibacterial and Wound Healing Properties. *Biocatal. Agric. Biotechnol.*, **2025**, *67*, 103688.
44. D. Dinga, A. Ekennia, C. U. Ogbonna, D. A. Udu, D. M. N. Mthiyane, U. Marume and D. C. Onwudiwe, *Sci. Afr.*, **2022**, *17*, e01366.
45. H. Hemmami, I. B. Amor, S. Zeghoud, S. E. Laouini, E. Nleonu, P. Pohl and J. Simal-gandara, *J. Turk. Chem. Soc. Sect. Chem.*, **2024**, *11*(2), 731–750.
46. Z. E. Radhi and N. O. Jasim, *IOP Conf. Ser. Earth Environ. Sci.*, **2021**, *790*, 012089.
47. S. Stankic, M. Müller, O. Diwald, M. Sterrer, E. Knözinger and J. Bernardi, *Angew. Chem. Int. Ed.*, **2005**, *44*, 4917.
48. F. Aziz, A. B. Gulshan, Z. Usman, M. Rehman, Q. Khalid, M. N. Khan, M. U. Munir, H. T. Masood and M. Rafique, *Results Chem.*, **2025**, *1*, 102248.
49. E. Saied, A. M. Eid, S. E. D. Hassan, S. S. Salem, A. A. Radwan, M. Halawa, F. M. Saleh, H. A. Saad, E. M. Saied and A. Fouda, *Catalysts*, **2021**, *11*, 821.
50. N. Baghban, M. Jamali, S. Pourfadakari, S. Dobaradaran and N. Yusefi, *Chem. Eng. Commun.*, **2025**, *212*, 157–173.
51. D. M. Radulescu, I. A. Neacsu, B. S. Vasile, V. A. Surdu, O. C. Oprea, R. D. Trusca, C. Chircov, R. C. Popescu, C. I. Ilie, L. M. Ditu and V. Drumea, *Int. J. Mol. Sci.*, **2025**, *26*, 9021.
52. A. H. Obead and N. K. Abbas, *Baghdad Sci. J.*, **2025**, *22*, 2638–2646.
53. R. Sreekanth, J. Pattar, A. V. Anupama and A. M. M. Mallikarjunaswamy, *Appl. Phys. A*, **2021**, *127*(10), 797.
54. S. Vijayakumar, V. N. Punitha and N. Parameswari, *Arab. J. Sci. Eng.*, **2022**, *47*(6), 6729–6734.
55. S. Sagadevan, J. A. Lett, I. Fatimah, K. T. Selvi, R. P. Sivasankaran, G. K. Weldegebrieal and W. C. Oh, *Processes*, **2022**, *10*(10), 2098.
56. P. Yadav, R. Saini and A. Bhaduri, *Environ. Sci. Pollut. Res.*, **2023**, *30*(28), 71439–71453.
57. Z. M. Alaizeri, H. A. Alhadlaq, S. Aldawood, M. J. Akhtar, M. S. Amer and M. Ahamed, *Nanomater.*, **2021**, *11*(11), 2915.
58. D. M. Radulescu, I. A. Neacsu, B. S. Vasile, V. A. Surdu, O. C. Oprea, R. D. Trusca, C. Chircov, R. C. Popescu, C. I. Ilie, L.M. Ditu and V. Drumea, *Int. J. Mol. Sci.*, **2025**, *26*(18), 9021.
59. R. Dobrucka, *Iran. J. Sci. Technol., Trans. A, Sci.*, **2018**, *42*(2), 547–555.
60. R. B. Rotti, D. V. Sunitha, R. Manjunath, A. Roy, S. B. Mayegowda, A.P. Gnanaprakash, S. Alghamdi, M. Almehmadi, O. Abdulaziz, M. Allahyani. and A. Aljuaid, *Front. Chem.*, **2023**, *11*, 1143614.
61. S. Abinaya and H. P. Kavitha, *ACS omega*, **2023**, *8*(6), 5225.
62. K. Mageshwari, S. S. Mali, R. Sathyamoorthy and P. S. Patil, *Powder Technol.*, **2013**, *249*, 456–462.
63. H. T. Sim, M. Gençaslan and M. Merdan, *Discov. appl. sci.*, **2024**, *6*, 577.
64. L. Todan, L. Predoană, G. Petcu, S. Preda, D. C. Culiță, A. Băran, R. D. Trușcă, V. A. Surdu, B. S. Vasile and A. C. Ianculescu, *Gels*, **2023**, *9*, 624.
65. V. Soleimanian and S. R. Aghdaee, *J. Phys. Chem. Sol.*, **2015**, *81*, 1–9.
66. W. M. Girma, M.S. Aragie, B. A. Berehe and A. H. Assen, *Mater. Adv.*, **2025**, *6*, 4003–4015.
67. M. A. Ammulu, K. V. Viswanath, A. K. Giduturi, P. K. Vemuri, U. Mangamuri and S. Poda, *J. Genet. Eng. & Biotechnol.*, **2021**, *19*, 21.
68. A. Akshaykranth, N. Jayarambabu, V. R. Tumu and R. K. Rajaboina, *J. Inorg. Organomet. Polym. Mater.*, **2021**, *31*, 2393–2400.
69. R. Wahab, S, G. Ansari, M. A. Dar, Y. S. Kim and H. S. Shin, *Mater. Sci. Forum*, **2007**, 558, 983–986.
70. F.Aziz, A. B. Gulshan, Z. Usman, M. Rehman, Q. Khalid, M. N. Khan, M. U. Munir, H. T. Masood and M. Rafique, *Results Chem.*, **2025**, *15*, 102248.
71. W. M. Girma, M. S. Aragie, B. A. Berehe and A. H. Assen, *Materials Advances*, **2025,** *6*, 4003–-4015.
72. A. Sajid, J. Zahid, A. Sajid, N. Shaukat, F. Nadeem, Q. Manzoor and A. Ahmad, *WASTE BIOMASS VALORI.*, **2025**, 1–16.
73. A. O. Manaa, H. H. Baghdadi, L. A. Heikal and L. S. El-Hosseiny, *Sci. Rep.*, **2025**, *15*, 32484.
74. M. K. Soliman, A. H. Talib, R. Mahmoud, Z. A. Ali, H. H. Al-Haideri, A. Abalkhail, A. S. Binshaya, M. H. Salem, F. O. Al-Otibi and M. T. Yassin, *AMB Express*, **2025**, *15*, 1–20.
75. A. Muhaymin, H. E. A. Mohamed, K. Hkiri, A. Safdar, S. Azizi and M. Maaza, *Sci. Rep.*, **2024**, *14*, 20135.
76. M. K. Patel, V. V. Agrawal, B. D. Malhotra and S. J. M. F. Ansari, *Mater. Focus*, **2014**, *3*, 1